Experiments in Fluids
August 2017, Volume 58 Issue 8 Pages 104 (1-9)
http://dx.doi.org/10.1007/s00348-017-2383-1
http://archimer.ifremer.fr/doc/00392/50315/

Visualization of the contact line during the water exit of flat plates

Tassin Alan [1, *], Breton Thibaut [1, 2], Forest Bertrand [1], Ohana Jeremy [1], Chalony Sebastien [1], Le Roux Dominique [1], Tancray Aurelien [1]

[1] IFREMER,Plouzané,France
[2] ENSTA Bretagne,FRE CNRS 3744, IRDLBrest Cedex 09,France

* Corresponding author : Alan Tassin, email address : alan.tassin@ifremer.fr

Abstract :

We investigate experimentally the time evolution of the wetted surface during the lifting of a body initially floating at the water surface. This phenomenon is referred to as the water exit problem. The water exit experiments were conducted with transparent (PMMA) mock-ups of two different shapes: a circular disc and a square flat plate. Two different lighting systems were used to diffuse light in the mock-up material: a central high-power LED light normal to the surface and an edge-lighting system featuring an array of LED lights. These setups make it possible to illuminate the contact line, which delimits the surface of contact between the mock-up and the water. The characteristic size of the mock-ups is about 20 cm and the acceleration of the mock-up oscillates between 0 and 25 m/s2. We show that the central light setup gives satisfactory results for the circular disc and that the edge lighting technique makes it possible to follow a contact line with a time-evolving complex shape (strong changes of convexity) up to 1000 fps. The observations presented in the paper support the possibility of extending this promising technique to more general three-dimensional bodies with arbitrary motion (e.g., including pitch motion).

1 Introduction

The water exit problem, or the lifting of a body initially floating at the water surface, has regained attention and motivated a number of studies in the last years. In most applications, the water exit problem is associated with the water entry problem. In that case, one will speak about an exit stage which is most of the time subsequent to an entry stage. In marine applications such as wave impact on a horizontal platform (Baarholm and Faltinsen 2004), ship slamming (Kaplan 1987) or wave impact on suspended structures (Sun and Helmers 2015), the water entry and exit event is due to the relative motion between the body and the free surface. The aeronautical industry has to deal with the water entry and exit of a body whose shape varies in time when using a 2D+t approach (also known as strip theory) for the prediction of the hydrodynamic loads on the fuselage during emergency landing on water (Tassin et al. 2013). In contrast to the extensive research on the water entry problem, which has lead to different linear and nonlinear Wagner-type models, much less work has been dedicated to the water exit problem. To the best of our knowledge, except the experiments reported by Reis et al. (2010), most of the investigations on water exit were performed numerically and analytically (ex: Sun and Helmers 2015; Korobkin 2013; Tassin et al. 2013). It is nevertheless worth mentioning the experimental work of Bourrier et al. (1984) and Truscott et al. (2016) on the 'pop-up' effect, although this water exit phenomenon is rather different because of the total initial immersion of the body. Among the questions raised by the modelling of the water exit stage, the evolution of the contact line remains a crucial and open question.

As a first step to a better understanding of the exit stage and assessment of the existing analytical model

of Korobkin (2013), we attempted to measure the evolution of the contact line, or the wetted surface. Unlike previous experimental work on water entry which showed that bottom views could be used to measure the evolution of the wetted surface on non-transparent three-dimensional mock-ups (see Halbout 2011; Takagi 2004), we observed a much poorer contrast between the wetted surface and the rest of the mock-up, so we decided to continue our investigations with a transparent mock-up. Scolan et al. (2006) previously used a transparent plate in order to study wave impacts on a fixed flat plate. In their experiments, they used a draughtboard placed at the bottom of the wave tank and a video camera above the mock-up. They discreminated the wetted surface from the rest of the transparent plate as the surface over which the bottom of the tank (the draughtboard) was visible. Instead of using the "draughtboard technique", which is probably difficult to use with curved three-dimensional bodies, complex body motions including pitch or in deep wavetanks, we aimed at illuminating the contact line. The draughtboard technique was nevertheless used to show that the results that we obtained from both techniques were in good agreement.

2 Experimental set-up

In the experimental set-up described in Fig. 1, the mock-up is held by high-stiffness strings which are connected to a rigid metallic frame. This frame is moved upwards (z-axis) by an electric translation actuator. A high-speed camera (Photron FastCam Mini AX50) records a top view of the mock-up. A second camera (Photron FastCam Ultima APX) was also used during specific experiments carried out with the circular disc in order to record simultaneaously side views and top views. Note that both cameras are fitted with a 100 mm lens. The lower face of the mock-ups is initially put in contact with the still water surface ($z = 0$) while minimising the penetration depth. Two different lighting systems have been tested : a central LED light (configuration 1) and a LED edge-lighting system (configuration 2).

2.1 Configuration 1 : central LED lighting

In configuration 1, a high-power LED light (Minostar LED-spot) is fixed at the centre of the mock-up as depicted in Fig. 1. The Minostar LED-spot has a viewing angle of 45°and a luminous flux of 140 lm. The upper surface of the mock-up located under the LED is roughened in order to facilitate the light diffusion in the PMMA. This configuration has been tested with a circular disc of radius 10 cm and thickness 8 mm and with a square plate of thickness 8 mm and side length of 20 cm. During the experiments, the acceleration was measured with an accelerometer fixed on top of the LED in order to analyse more precisely the motion undergone by the mock-up. A record obtained during the water exit of the circular disc is plotted in Fig. 2. One can see that the acceleration of the mock-up exhibits significant variations which can be imputed to the compliance of the strings of the set-up. As far as we are concerned with showing the feasibility of the visualisation technique, one can consider that the different mock-ups undergo approximately the same time evolution as the record plotted in Fig. 2 (in terms of flow regime). The elevation of the mock-up was derived from the acceleration measurement via a double time integration of the acceleration signal. The elevation was used to compare the results obtained from different experiments at similar elevations.

2.2 Configuration 2 : LED edge-lighting

In configuration 2, LED arrays were mounted at the periphery of a square plate of thickness 15 mm and a side length of 20 cm. In order to be able to incorporate LED lights without disturbing the water, the square plate was continued obliquely with a slope of 30° as depicted in Fig. 3 which shows a vertical cross-section of the mock-up. Note that the thickness of the extrapolated sides was set to 12 mm in order to avoid any masking of the lower face from the camera point of view. Altogether, the 4 LED arrays (SMD 5050 EPISTAR) supply a luminous flux of about 1000 lm. The edges of the mock-up in contact with the LEDs, which have a viewing angle of 120°, were also roughened to homogenize the light diffusion in the PMMA.

3 Results

In this section, we present the results obtained with the different techniques. All the images depicted in this section were captured at a frame rate of 1000 fps. Note that the online version of the article offers the possibility of zooming in on small details of the images.

3.1 Top view of the circular disc - Configuration 1

A sequence of 4 images for different elevations, $h(t)$, obtained during the water exit of the circular plate with configuration 1 is plotted in Fig. 4. The acceleration

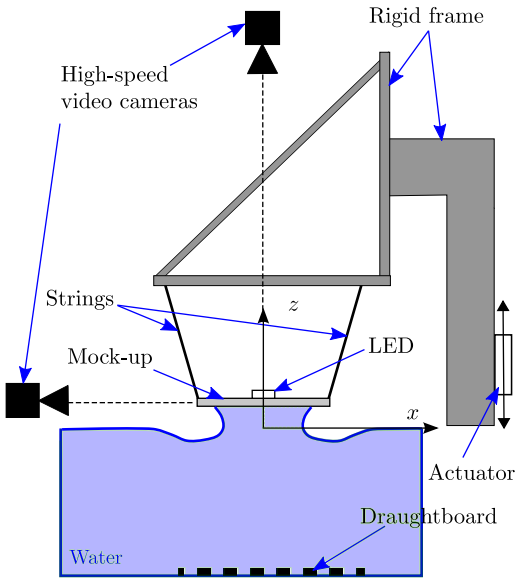

Fig. 1: Description of the experimental set-up

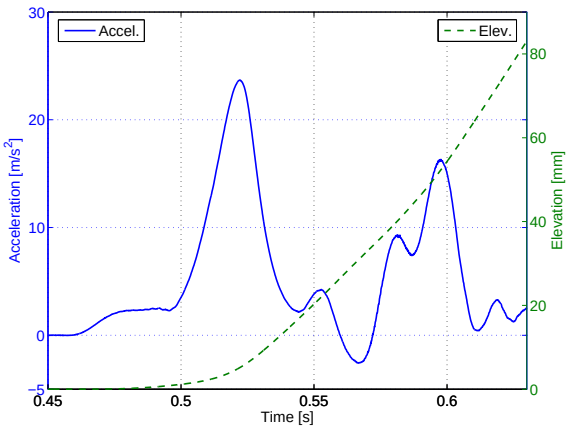

Fig. 2: Acceleration and elevation during the water exit of a circular disc

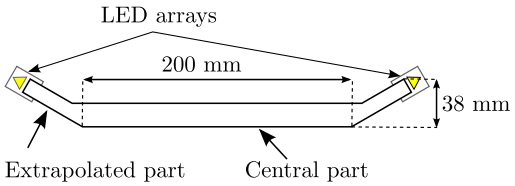

Fig. 3: Description of the edge-lighting configuration (Configuration 2) for a square plate

and elevation during this test are the same as in Fig. 2. One can see that an inner ring appears inside the outer ring corresponding to the periphery of the disc. The inner ring follows the contact line : it appears at the periphery of the disc and contracts towards the centre as the mock-up exits the water. Despite the imperfections of the mechanical system holding the mock-up (the mock-up is held by 3 strings), the contact line remains closely circular during the exit. Note that the intensity of the light increases significantly as the contact line approaches the light source. In order to check that the ring of light visible in Fig. 4 corresponds to the contact line (boundary of the wetted surface), we carried out experiments with a draughtboard at the bottom of the water tank (about 40 cm under the water surface), allowing a direct visualisation of the contact surface. A sequence of images of a test with a draughtboard is presented in Fig. 5. Note that the elevation corresponding to the different images of Fig. 5 are very close to the elevation corresponding to the images of Fig. 4. One can see that the region over which the draughtboard is visible and undeformed follows the same evolution as the ring of light visible in Fig. 4. In fact, this ring is clearly visible at the periphery of the draughtboard surface in Figs. 5c and 5d. This comparison is however less obvious in Figs. 5a and 5b due to the smaller contrast between the contact line and the image background.

In order to allow for a better comparison between the two techniques, the geometry of the contact line observed in Fig. 4 was extracted. The contour detection algorithm that we used is based on the Taubin method (Taubin 1991) and the shape of the contact line was assumed to be elliptic. The perfomance of the contour detection algorithm is illustrated in Fig. 6, where the elliptic contours obtained with this approach have been superimposed to the original images. These elliptic contours were also superimposed to the images obtained from the draughtboard technique, as plotted in Fig. 7. Although the elevations of Figs. 5 and 4 are very close, the parameters of the ellipse measured from the images of Fig. 4 were interpolated linearly between the time steps in order to improve the comparisons between the two experiments. One can clearly see that the regions overwhich the draughtboard is undistorted is delimited by a contour closely related to the elliptic contour extracted from Fig. 4, thus demonstrating the accuracy of the contour illumination technique. Although the overall agreement is very satisfactory, one can observe some discrepancies due to the imperfections of the set-up (e.g. the mock-up rotates slightly) when zooming very close to the contact line (the online version offers the possibility of zooming close to the contact line).

For these experiments, the aperture of the lens was adjusted such that both the mock-up and the draughtboard were reasonnably well in focus and such that the aperture of the diaphragm was not too small in order to be able to see the contact line which is much less luminous than the draughtboard. The contrast of the images presented in Figs. 4 - 7 was adjusted numerically in order to make the contact line more visible.

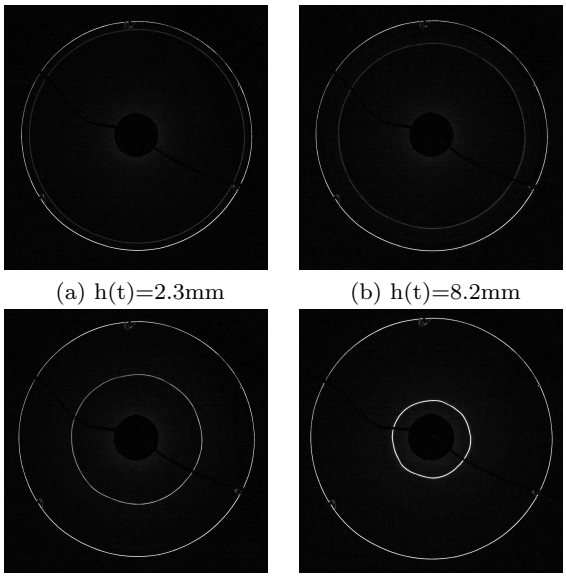

(a) h(t)=2.3mm (b) h(t)=8.2mm

(c) h(t)=30.4mm (d) h(t)=60.8mm

Fig. 4: Configuration 1 : image sequence of the contact line for a circular disc (see online version for high definition images)

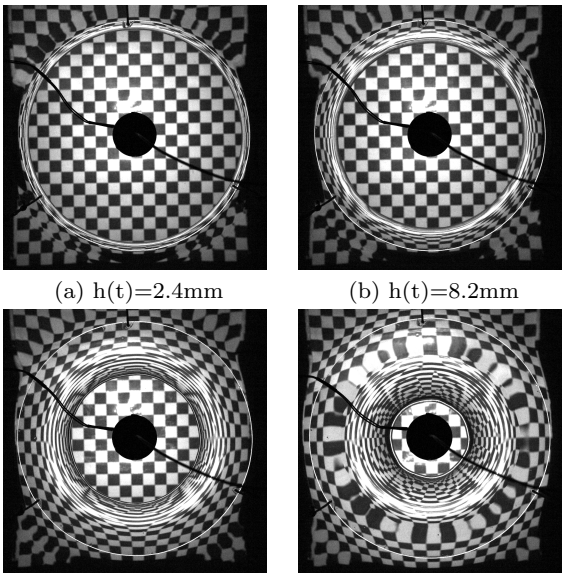

(a) h(t)=2.4mm (b) h(t)=8.2mm

(c) h(t)=30.3mm (d) h(t)=60.6mm

Fig. 5: Configuration 1 with draughtboard (see online version for high resolution images)

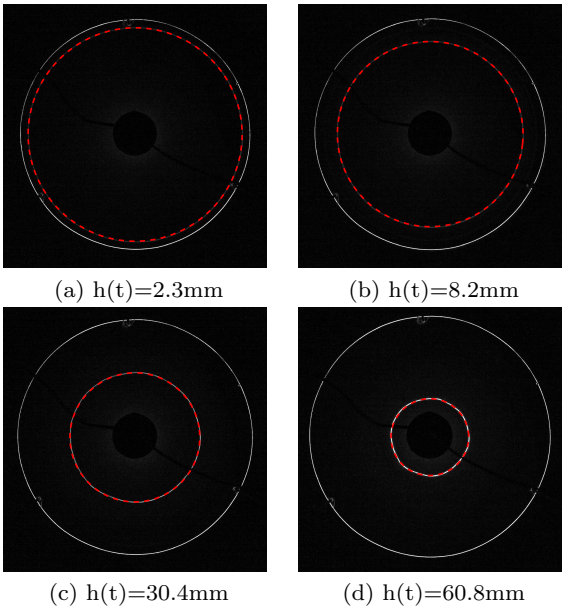

(a) h(t)=2.3mm (b) h(t)=8.2mm

(c) h(t)=30.4mm (d) h(t)=60.8mm

Fig. 6: Detection of the contact line for a circular disc (see color version online)

3.2 Side views of the circular disc

In order to assess the accuracy of the draughtboard technique and the contact line illumination technique, we performed experiments during which we recorded simultaneously side views and top views (with two cameras). We added a white background in order to visualize the water column by shadowgraphy. Figs. 8 and 9 show the shape of the water column which rises under the circular plate for different values of the elevation. These images were obtained during three different experiments and correspond to the time instant when perspective effects are minimal. From these images, we measured the diameter, ϕ_c, of the water column where its horizontal cross-section is minimal and the diameter of the disc, D_s, as depicted in Fig. 9. The diameter ϕ_c also corresponds to the point where the tangent to the free surface is vertical. In the following comments and throughout the rest of the paper, the portion of the free surface located above the point where the tangent of the free surface is vertical will be referred to as the "meniscus region" and the portion of the free surface located below this point/line will be referred to as the "water column". From the top views, we measured the diameter of the luminous ring, ϕ_r, the diameter of the draughtboard area, ϕ_d, and the diameter of the disc, D_t,

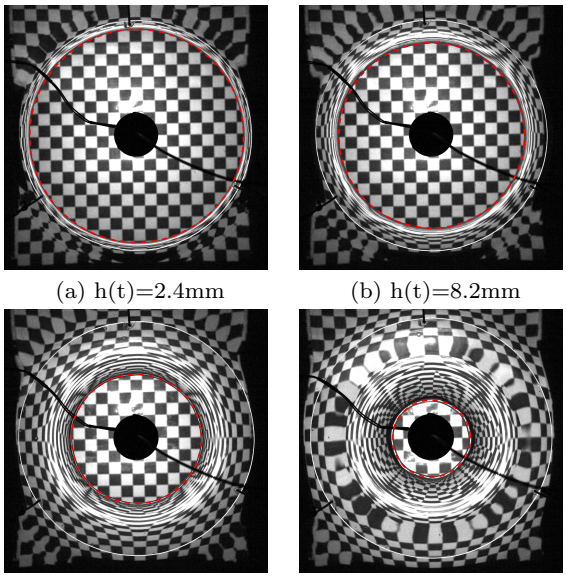

(a) h(t)=2.4mm (b) h(t)=8.2mm

(c) h(t)=30.3mm (d) h(t)=60.6mm

Fig. 7: Comparison between the detected contact line and the draughtboard technique for a circular disc (see color version online)

as depicted in Fig. 10. Note that Fig. 10 corresponds to the same experiment and to the same time instant as Fig. 9. A zoomed in view of the regions delimited by the red square boxes depicted in Fig. 10 is shown in Fig. 11. One can see on this figure that the diameter of the luminous ring is slightly greater than the diameter of the draughtboard. In a similar way, zoomed in views of the regions marked by red dotted circles in Fig. 9 are shown in Fig. 12, where we have also plotted the left and right limits of the luminous ring and of the draughtboard which were measured from Fig. 10 or 11. This comparison confirms that the value of the diameter measured with the draughtboard technique, ϕ_d, is very close to the diameter of the water column, ϕ_c, measured from the side view. The luminous ring seems to be coincident with the region where the slope of the meniscus is approximately equal to 45°, so it does not correspond to a contact line strictly speaking. It should be noted that the disc remains fully wet until the end of the exit as a thin film of water remains at its surface. In water entry problems, the name "contact line" or "turn over" region designates the curve where the free surface is vertical (see Korobkin 2007). Although a wider surface of the body surface is wet by the jet, the surface of the body delimited by "the contact line" is often referred to as the "wetted surface" or the "contact surface". It seems therefore consistent to use the same terminology for the water exit problem and to use the name "contact line" for the "turn over line" of diameter ϕ_c indicated in Fig. 9. A compilation of the measurements obtained from the different experiments is presented in table 1. The results are given in terms of average values over four consecutive experiments. In the notations, the overline stands for the average value of four experiments and $\overline{(X-Y)}$ stands for the average value of $(X-Y)$ over four experiments, so $\overline{(X-Y)} \neq (\overline{X}-\overline{Y})$. Two different series of experiments had to be conducted in order to measure ϕ_d (with the draughtboard) and ϕ_r (without the draughtboard) at an elevation of $h(t) \approx 9.5$mm. This is why the results for $h(t) \approx 9.5$mm appear on two different lines in Tab. 1. The results shown in Tab. 1 confirm that ϕ_c and ϕ_d are very close throughout the exit and that ϕ_r is slightly greater than ϕ_c by a few percents. From a practical point of view, it is therefore reasonnable to consider that the illumination technique gives a good measurement of the contact line. Note that the difference between ϕ_r and ϕ_c is smaller for smaller values of $h(t)$, probably because the meniscus is smaller at the beginning of the exit. This a valuable point as the highest hydrodynamic loads appear when the wetted surface is large in a number of water exit configurations (e.g. water exit at constant acceleration (Korobkin 2013) , wave impact (Baarholm and Faltinsen 2004), water entry and exit at constant acceleration (Tassin et al. 2013)).

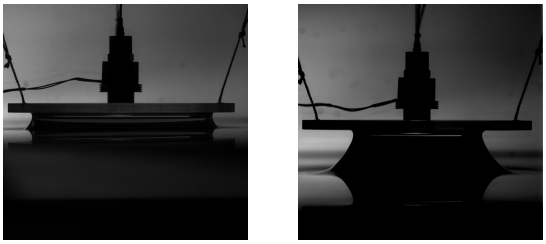

(a) h(t)=9.5mm (b) h(t)=30.1mm

Fig. 8: Side view of a disc exiting water

3.3 Square plate - Configuration 1

The central LED lighting technique was also used to study the water exit of a square plate. For this particular case, some sellotape was stuck to the lower face of the plate under the LED light in order to reduce the light transmission into the water and to increase the light diffusion in the material of the mock-up (the sellotape acts as a mirror). Three images recorded during the water exit of a square plate are plotted in Figs. 13a-13c, showing a more complex evolution of the contact line. The contraction of the contact surface is slower

$\overline{h(t)}$ (mm)	$\overline{\phi_c/D_s}$ (%)	$\overline{\phi_d/D_t}$ (%)	$\overline{\phi_r/D_t}$ (%)	$\overline{(\phi_d/D_t - \phi_c/D_s)}$ (%)	$\overline{(\phi_r/D_t - \phi_c/D_s)}$ (%)
9.12	80.1	79.8	-	-0.25	-
9.75	79.5	-	79.8	-	0.36
30.1	55.3	55.1	56.2	-0.14	0.91
41.9	44.6	44.4	45.5	-0.22	0.87

Table 1: Average values of the relative diameters for 4 different elevations. The overline stands for the average on 4 consecutive experiments. (D_s: diameter of the disc measured from the side view, ϕ_c: minimum diameter of the water column measured from the side view, D_t: diameter of the disc measured from the top view, ϕ_d: diameter of the undeformed draughtboard surface, ϕ_r: diameter of the luminous ring)

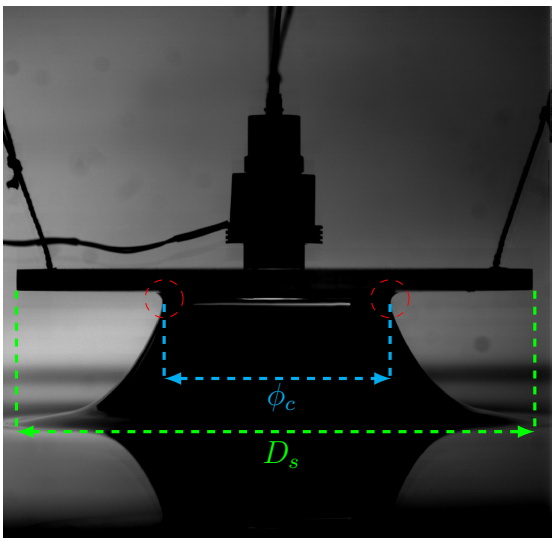

Fig. 9: Side view of a disc at h(t)=42.3mm

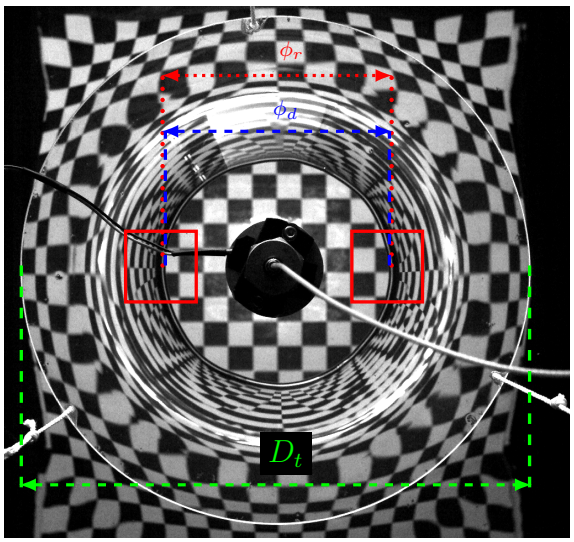

Fig. 10: Top view of the disc with the draughtboard and central LED light at h(t)=42.3mm

along the diagonals of the square. At the end of the exit, the contact surface is very elongated along the diagonals. Note that the luminosity of the contact line is more intense in the regions where the light source incidence is normal to the contact line (this was supported by additional observations not presented in the paper). It was necessary to increase significantly the contrast of these images in order to be able to make the contact line entirely visible. Fig. 13d was obtained from another experiment during which a draughtboard was placed under the right-hand side of the mock-up. This image allows for a side by side comparison with Fig. 13c, given that the elevations corresponding to these two images are very close. Note that the draughtboard is visible in the thin elongated region of the contact surface along the diagonals in Fig. 13d. This confirms that the contact surface is very elontaged in these regions and indicates that the water column also has a complex shape. Also note the apparition of the draughtboard on the left-hand side of the image, probably due to refraction through the free surface. As the sellotape kept the LED light from being transmitted to the water,

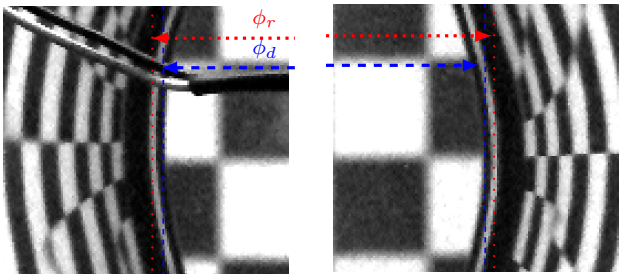

(a) Left (b) Right

Fig. 11: Zoomed in views of Fig. 10

we used underwater lights to lighten the draughtboard in this experiment.

3.4 Modified square plate - Configuration 2

Based on the previous observations, we tried to improve the results using the LED edge-lighting system described in Fig. 3. While increasing the global luminous flux, this set-up aimed at having a wider distribution of the light source. In that way, each portion of

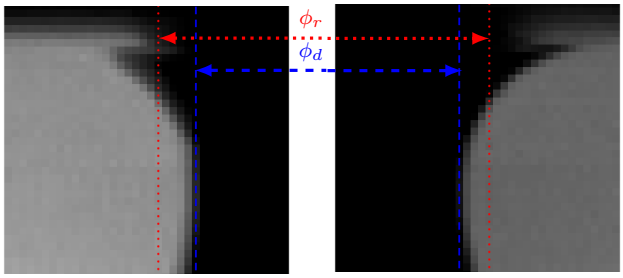

(a) Left (b) Right

Fig. 12: Zoomed in views of Fig. 9 with measurements from Fig. 11 superimposed

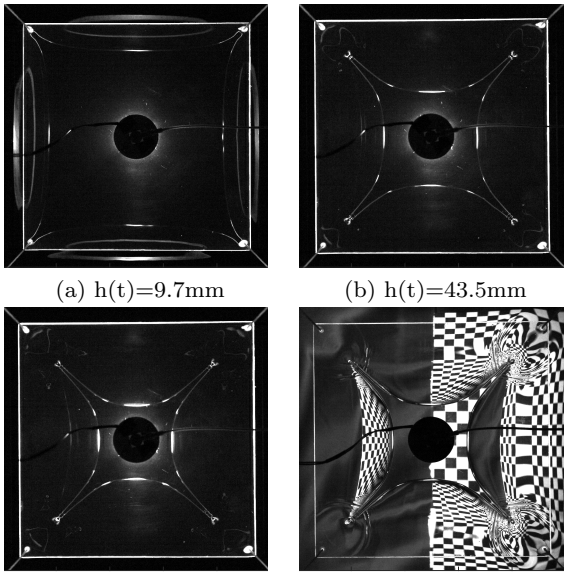

(a) h(t)=9.7mm (b) h(t)=43.5mm

(c) h(t)=53.9mm (d) h(t)=53.6mm

Fig. 13: Configuration 1 : square plate with central LED. (a), (b) and (c) : experiment without draughtboard, (d) : experiment with a draughtboard.

the contact line is likely to receive sufficient light from any direction. A sequence of images obtained with configuration 2 for the modified square plate is shown in Fig. 14. One can observe that configuration 2 improves both the intensity and the homogeneity of the contact line illumination. In fact, it is still possible to make the contact line more visible in Fig. 14 whereas the signal-to-noise ratio of the images presented in Fig. 13 prevents from doing so. Note that the accelerometer fixed at the middle of the mock-up (slightly off-centre of the mock-up) is also visible in Fig. 14. The contact line remains reasonnably well in focus until an elevation of 60 mm, but it becomes noticeably out of focus when approaching an elevation of 100 mm in Fig. 14d. The same experiment has been carried out with a draughtboard which was located at the bottom of the tank and illuminated by an under water lighting system. During this experiment, the LED edge-lighting system was also switched on. The images obtained with this configuration are depicted in Fig. 15. In order to offer a better comparison between Figs. 14 and 15, we selected manually several points "belonging" to the contact line in the images of Fig. 14 and superimposed these points (red crosses) to the images of Fig. 15. This comparison clearly shows that the contact line extracted from Fig. 14 is very close to the curve delimiting the surface overwhich the draughtboard is visible. The contact line illuminated by the LED edge-lighting system is also visible in Figs. 15c and 15d, especially when zooming in on the regions where the contact line is close to the centre of the mock-up. The contact line is also visible in Fig. 13d, together with the draughtboard, in the regions close to the central LED light. Zoomed in views of Figs. 13d and 15c are presented in Figs. 16a and 16b in order to compare more precisley the two techniques at similar elevations. It is interesting to observe that there is a gap between the border of the draughtboard and the contact line with both techniques, although the direction of propagation of the incident light with respect to the contact line is reversed. In configuration 1 the light comes from the centre of the wetted surface towards the contact line whereas in configuration 2 the light comes from outside of the wetted surface towards the contact line. The size of this gap seems however to be of the same order of magnitude in both cases. More importantly, the difference between the contact line illumination techniques and the draughtboard technique remains small, even for large elevations of about 54 mm.

4 Discussion

The results obtained with the circular disc show that the draughtboard technique is a reliable technique for the measurement of the minimum diameter of the water column which can be measured from side views. These measurements were made by selecting manually, from zoomed in views of the images, the limits of the features that we wanted to measure (ϕ_c, ϕ_r, ϕ_d ...). As pointed out by Vega et al. (2009), such measurements are not that simple. We showed that the contact line obtained with the central LED light and the wetted surface obtained with the draughtboard technique superimpose well both for the circular disc and the modified square plate. These comparisons are better when we compare images obtained at similar elevations (as shown in the paper) than when we compare images obtained at similar "time instants". In fact, besides the

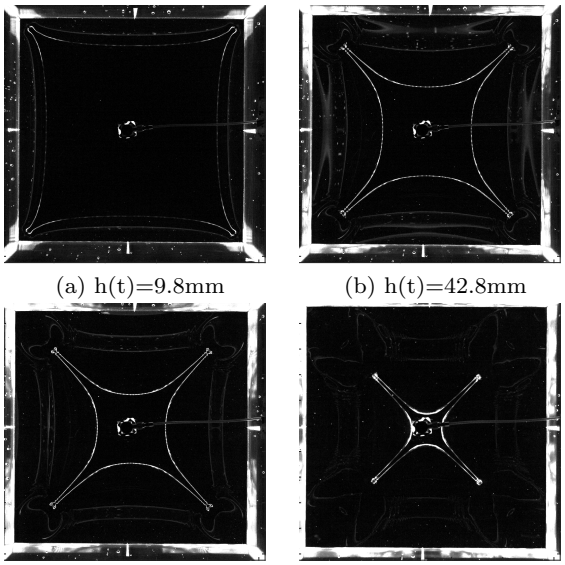

(a) h(t)=9.8mm (b) h(t)=42.8mm

(c) h(t)=54.1mm (d) h(t)=94.5mm

Fig. 14: Configuration 2 : modified square plate with the LED edge-lighting system

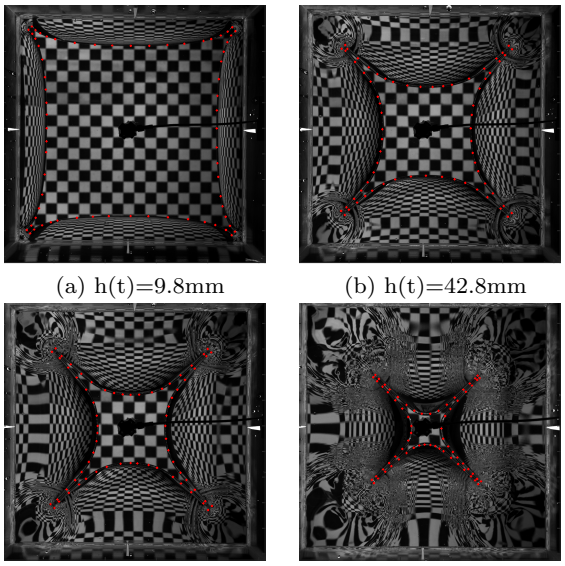

(a) h(t)=9.8mm (b) h(t)=42.8mm

(c) h(t)=54.2mm (d) h(t)=94.5mm

Fig. 15: Configuration 2 : modified square plate with the LED edge-lighting system. The red crosses indicate the location of points selected manually from the contact contact line in Fig. 14 (see HD color version online)

difficulty of finding a reference time for such comparisons, the discrepancies in terms of time evolution of the acceleration from test to test make these comparisons more difficult when they are based on time. We should also mention that we selected experiments which "matched" rather well, but that some comparisons with other experiments were less satisfactory. These discrepancies probably come from the imperfections of the set-up (the mock-up is held by strings) and the discrepancies in terms of time evolution of the acceleration from test to test. The overall accuracy of the comparisons is nevertheless sufficient to support the conclusions drawn from the different experiments. Note that the comparisons between the side views and the top views, which were performed on the same experiments, are less affected by the test-to-test variations of the experimental conditions (acceleration).

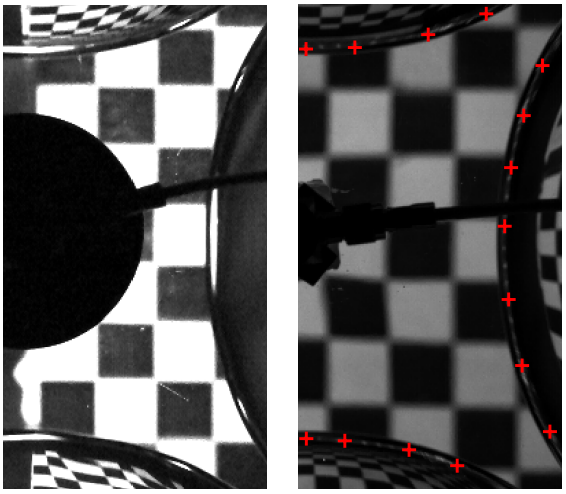

(a) h(t)=53.6mm (b) h(t)=54.2mm

Fig. 16: Zoomed in views of the contact line during the water exit of a square plate with (a) the central LED lighting and (b) the LED edge-lighting system (see HD color version online)

The results show that configuration 2 improves significantly the illumination of the contact line during the water exit of a square plate. This configuration was tested because we intuited that the illumination of the contact line could be influenced by the angle of incidence of the incident light with respect to the contact line normal/tangent. The parameters affecting the optical phenomenon are however not yet fully identified. For example, one can see in Fig. 13a that the thin tips of the contact line along the diagonals of the square plate are clearly visible although the contact line is NOT orthogonal to the incident light. We were not able to show whether the sides of the plate play a role in that illumination. Another interesting aspect is the fact that the contact line is illuminated both when the light comes from the centre of the mock-up and from the periphery of the mock-up.

5 Conclusion and perspectives

The LED edge-lighting technique proposed for the visualisation of the innermost point of the contact line during water exit is promising. It allows for an intense and homogeneous illumination of the innermost point of the contact line. The feasability of the method was proven by carrying out experiments at 1000 fps with a modified square plate. The performance is remarkable given the complexity of the shape of the contact line. The draughtboard technique was used to show the close correspondance between the illuminated contact line and the undeformed part of the draughtboard. The proposed method could potentially be extended to more complex case studies: three-dimensional bodies and bodies subject to more complex motions including rotations (the camera should be fixed to the mock-up in that case), maybe with some restrictions on the curvature and the deadrise angle (slope of the tangent) of the mock-up. This technique is also worth investigating for the tracking of contact lines in different configurations (e.g. along a wall, sloshing and water entry problems). Numerical simulations of the optical phenomenon would certainly be helpfull to better understand the interaction between the contact line (or the meniscus) and the lighting system. Such an analysis might require a more accurate measurement of the free surface shape around the meniscus region in order to be able to understand accurately the phenomenon. This type of measurement is already challenging in the axisymetric case and probably out of reach for more complex cases like the square plate. An alternative solution would be to use numerical simulation to obtain a realistic shape of the free surface, provided that these results are reliable.

Acknowledgements

The authors would like to thank Dr Nicolas Jacques and Dr Aboulghit el Malki Alaoui from ENSTA Bretagne for lending the Photron FastCam Ultima APX and the interesting discussions that followed the experiments. The first author would also like to thank Florent Colas and Morgan Tardivel from IFREMER for their advice on the optical aspects of the set-up.

References

Baarholm, R. and Faltinsen, O. M. (2004). Wave impact underneath horizontal decks. *Journal of Marine Science Technology*, 9:1–13.

Bourrier, P., Guyon, E., and Jorre, J. (1984). The 'pop off' effect: different regimes of a light ball in water. *European Journal of Physics*, 5(4):225.

Halbout, S. (2011). *Contribution à l'étude des interactions fluide-structure lors de l'impact hydrodynamique avec vitesse d'avance d'un système de flottabilité d'hélicoptère*. PhD thesis, Université d'Aix-Marseille, France.

Kaplan, P. (1987). Analysis and prediction of flat bottom slamming impact of advanced marine vehicles in waves. *International Shipbuilding Progress*, 34(391):44–53.

Korobkin, A. (2007). Second-order wagner theory of wave impact. *Journal of Engineering Mathematics*, 58(1-4):121–139.

Korobkin, A. A. (2013). A linearized model of water exit. *Journal of Fluid Mechanics*, 737:368–386.

Reis, P. M., Jung, S., Aristoff, J. M., and Stocker, R. (2010). How cats lap: Water uptake by felis catus. *Science*, 330:1231–1234.

Scolan, Y., Remy, F., and Thibault, B. (2006). Impact of three-dimensional standing waves on a flat horizontal plate. In 21^{st} *Workshop on Water Waves and Floating Bodies*, 2-5 April 2006, Loughborough, U.K.

Sun, H. and Helmers, J. B. (2015). Slamming loads on a wedge elastically suspended on a marine structure. In *ASME 2015 34th International Conference on Ocean, Offshore and Arctic Engineering*. American Society of Mechanical Engineers.

Takagi, K. (2004). Numerical evaluation of three-dimensional water impact by the displacement potential formulation. *Journal of Engineering Mathematics*, 48:339–352.

Tassin, A., Piro, D. J., Korobkin, A. A., Maki, K. J., and Cooker, M. J. (2013). Two-dimensional water entry and exit of a body whose shape varies in time. *Journal of Fluids and Structures*, 40:317–336.

Taubin, G. (1991). Estimation of planar curves, surfaces, and nonplanar space curves defined by implicit equations with applications to edge and range image segmentation. *IEEE Transactions on Pattern Analysis and Machine Intelligence*, 13(11):1115–1138.

Truscott, T. T., Epps, B. P., and Munns, R. H. (2016). Water exit dynamics of buoyant spheres. *Physical Review Fluids*, 1(7):074501.

Vega, E., Montanero, J., and Fernández, J. (2009). On the precision of optical imaging to study free surface dynamics at high frame rates. *Experiments in fluids*, 47(2):251–261.